nature portfolio

https://doi.org/10.1038/s41586-021-03879-4

Supplementary information

Inter-cellular CRISPR screens reveal regulators of cancer cell phagocytosis

In the format provided by the authors and unedited

Inter-cellular CRISPR screens reveal regulators of cancer cell phagocytosis

Roarke A. Kamber[1], Yoko Nishiga[1,2,3], Bhek Morton[1], Allison M. Banuelos[4,5,6], Amira A. Barkal[4,5,6,7], Felipe Vences-Catalán[8], Mingxin Gu[1], Daniel Fernandez[9,10], Jose A. Seoane[6,11], David Yao[1], Katherine Liu[1], Sijie Lin[1], Kaitlyn Spees[1], Christina Curtis[1,6,11,12], Livnat Jerby-Arnon[1,13], Irving L. Weissman[4,5,6,14], Julien Sage[1,2,6,9], Michael C. Bassik[1,6,9]*

1. Department of Genetics, Stanford University School of Medicine, Stanford, CA, USA
2. Department of Pediatrics, Stanford University School of Medicine, Stanford, CA, USA
3. Department of Radiation Oncology, Stanford University School of Medicine, Stanford, CA, USA
4. Institute for Stem Cell Biology and Regenerative Medicine, Stanford University School of Medicine, Stanford, CA, USA.
5. Ludwig Center for Cancer Stem Cell Research and Medicine, Stanford University School of Medicine, Stanford, CA, USA.
6. Stanford Cancer Institute, Stanford University School of Medicine, Stanford, CA, USA
7. Stanford Medical Scientist Training Program, Stanford University, Stanford, CA, USA.
8. Division of Oncology, Department of Medicine, Stanford University School of Medicine, Stanford, CA, USA.
9. Program in Chemistry, Engineering, and Medicine for Human Health (ChEM-H), Stanford University, Stanford, CA, USA
10. Stanford ChEM-H, Macromolecular Structure Knowledge Center, Stanford University, Stanford, CA, USA
11. Department of Medicine, Stanford University School of Medicine, Stanford, CA, USA
12. Program in Cancer Biology, Stanford University School of Medicine, Stanford, CA, USA
13. Chan Zuckerberg Biohub, San Francisco, CA 94158, USA
14. Department of Pathology, Stanford University School of Medicine, Stanford, CA, USA
*Correspondence to bassik@stanford.edu

Supplementary Information Contents:

Supplementary Notes

Supplementary Note 1. Development and analysis of CRISPRko ADCP screens

To establish a scalable platform for genetic screening in a macrophage-cancer cell co-culture system (**Fig. 1a**), we introduced Cas9 and a genome-wide CRISPR knockout library containing 10 sgRNAs targeting every protein-coding gene[1] into Ramos B-cell lymphoma cells, whose uptake by macrophages is stimulated by rituximab (anti-CD20) (**Extended Data Fig. 1a**). As a source of macrophages, we selected the macrophage cell line J774 because it exhibits high rates of cancer cell phagocytosis[2] (**Extended Data Fig. 1b**), and can be both readily cultured at scales (>10^{10} cells) necessary for robust genome-wide screens and efficiently manipulated genetically. The Ramos genome-wide knockout pool was subjected to two rounds of killing by LPS-activated macrophages, which exhibited higher ADCP than untreated macrophages (**Extended Data Fig. 1c,d, Supplementary Table 1**), in the presence of anti-CD20 mAbs. By sequencing the population of sgRNAs in the treated and untreated cell populations, we identified genes whose deletion increases or decreases Ramos cell abundance following treatment with macrophages and anti-CD20 (**Fig. 1b, Extended Data Fig. 1e, Supplementary Table 2**)

Supplementary Note 2. Development and analysis of CRISPRa ADCP screens

To enable CRISPRa screening in Ramos cells, we stably transduced Ramos cells with a VPR CRISPRa construct (i.e. deactivated Cas9 fused to the transcriptional activator domains of Vp64, p65, and Rta)[3] (**Extended Data Fig. 2a**) and a genome-wide activation library again containing 10 sgRNAs targeting each protein-coding gene[4]. We subjected the Ramos activation library to two rounds of selection by macrophages using the same screening strategy. Analysis of the screen revealed a large number of both anti-phagocytic hits (i.e. genes whose overexpression increases cell survival upon incubation with macrophages and anti-CD20 and anti-CD47 antibodies) and pro-phagocytic hits (**Fig. 1e, Extended Data Fig. 2b, Supplementary Table 4**). We noted that several of the sialic acid biosynthesis genes that scored as hits have been associated with immunosuppression but have unclear mechanistic roles in cancer progression. For example, *ST6GALNAC1* overexpression in cancer is known to generate the sialyl-Tn antigen, a well-known pan-carcinoma carbohydrate antigen associated with immunosuppressive microenvironment whose abundance is correlated with poor patient prognosis across a range of cancers[5,6]. *APMAP* was not detected as a hit, possibly because it is already expressed at high levels in Ramos cells.

Supplementary Note 3. Additional validation and control experiments for *APMAP*

Role of Fc receptor in APMAP-CD47 synergy

Anti-CD47 antibodies can induce phagocytosis via Fc-dependent and Fc-independent mechanisms, raising the question of whether an intact Fc domain is required for synergy between anti-CD47 and *APMAP* loss. We found that Fc receptor function was not required for synergy between *APMAP* deletion and anti-CD47 antibodies (**Extended Data Fig. 3e**), suggesting that the possible opsonizing effect of these antibodies is not required for *APMAP* loss to sensitize cells to phagocytosis. We also found that *APMAP* loss synergized with genetic deletion of *CD47* (**Extended Data Fig. 3f**), even in the absence of an antibody, further demonstrating that *APMAP* loss can synergize with the absence of *CD47* even in the absence of any opsonizing antibody.

Additional control experiments for APMAP

We confirmed that Karpas-299 cells were also sensitized to phagocytosis in the presence of anti-CD30 antibodies (**Extended Data Fig. 4a**) We monitored sensitivity of Ramos cells to phagocytosis driven by anti-CD20 mAbs in the presence of human U937 macrophages and observed that APMAP^{KO} cells were strongly sensitized to phagocytosis in the presence of antibodies, but not in the absence of antibodies (**Extended Data Fig. 4b**). We also confirmed that APMAP knockout cells were sensitized to ADCP in the presence of primary human peripheral blood monocyte-derived macrophages (**Extended Data Fig. 4c**). We also found that the effect of *APMAP* on ADCP susceptibility was not dependent on LPS treatment of macrophages (**Extended Data Fig. 4d**). We noted that cell surface levels of the canonical “eat-me” signals phosphatidylserine and calreticulin were comparable in Safe^{KO} and APMAP^{KO} cells (**Extended Data Fig. 4e**), suggesting that the increase in phagocytosis was not due to increase in a known “eat-me” signal. Additionally, we found that Ramos APMAP^{KO} cells did not exhibit altered cell surface levels of CD20 (**Extended Data Fig. 4f**), CD47 (**Extended Data Fig. 4g**), or sialic acids detected by lectin staining (**Extended Data Fig. 4h**). Ramos APMAP^{KO} cells also did not exhibit detectable differences in sensitivity to a panel of diverse cytotoxic agents (**Extended Data Fig. 4i**), or exhibit detectable alterations in cell size (**Extended Data Fig. 4j**), or in binding to macrophages in the presence of anti-CD20 across a range of concentrations (**Extended Data Fig. 4k**). The effect of *APMAP* on ADCP was not explained by any effects on lysosomal acidification, as *APMAP* loss also increased ADCP as measured using pH-independent dyes (**Extended Data Fig. 4l**). Thus, *APMAP* is a potent suppressor of ADCP in Ramos cells, but does not appear to operate through known ‘eat-me’ signals or by affecting binding of antibodies that induce ADCP.

Supplementary Note 4. Development of J774 screening platform

To establish and optimize a complementary genome-wide screening platform for ADCP regulators in J774 macrophages, we first conducted a genome-wide screen for uptake of IgG-opsonized 2.8 µm magnetic beads (**Extended Data Fig. 7a**). This screen identified numerous known positive and negative regulators of phagocytosis (consistent with our previous work[7]), including all members of the ARP2/3 and WAVE complexes, the Fc Receptor, and the Mac-1 integrin subunits[8], as well as many novel candidate phagocytosis regulators (**Extended Data Fig. 7b,c,d,e, Supplementary Table 6**). Though these beads differ greatly from cancer cells in terms of their size, stiffness, and surface composition, this proof of principle screen established that J774 macrophages can be used to robustly identify phagocytic regulators and surface receptors.

Supplementary Note 5. Discussion, limitations, and future directions

An important limitation of our study is that the experiments we conducted did not directly compare the potential of targeting *APMAP* with that of *CD47* or other anti-phagocytic factors. We nevertheless find that the effect of *APMAP* on tumour-targeting antibodies is preserved in vivo and in the context of a complex immune system. While there are known inter-species limitations to studying CD47 blockade in mice[9], our finding that *APMAP* loss enhances the anti-tumor effects not only of anti-CD47, but of rituximab and anti-TRP1 antibodies in mice, indicates that the effect of *APMAP* on tumour development is not limited to one particular antibody or tumour type. Further assessment of *APMAP* in additional pre-clinical models will be critical in evaluating its therapeutic promise in the context of different mAb therapies. While we identify GPR84 as critical for enhanced uptake of Ramos and Karpas-299 APMAP^{KO} cells by J774 macrophages in vitro, we did not evaluate the role of GPR84 in this process in vivo. Macrophages are known to express a large number of fatty acid binding GPCRs (such as FFAR1, FFAR2, FFAR3, FFAR4, HCAR3) that exhibit overlapping specificities, several of which were not detectably expressed in J774 macrophages (**Supplementary Table 1**). Further work will be required to determine whether other macrophage receptors are influenced by cancer-cell knockout of APMAP, and to what extent GPR84 contributes to control of APMAP^{KO} tumors in mice. Indeed, Nod mice were recently found to carry a putative loss of function allele of GPR84[10] so it may be that other factors are required for enhanced control of APMAP^{KO} tumours in those mice.

Surprisingly, unlike previously identified anti-phagocytic factors such as CD47 and CD24, in many cases *APMAP* loss on its own does not sensitize cancer cell lines to phagocytosis, but requires

the presence of tumour-targeting mAbs or CD47 blockade to induce phagocytosis. In other cases (such as with K562, HeLa, and B16-F10 cells), *APMAP* loss strongly enhances antibody-dependent phagocytosis but also sensitizes cells to phagocytosis in the absence of antibodies. The possible cancer-intrinsic factors that determine whether *APMAP* loss on its own is sufficient to sensitize cells to phagocytosis, as well as the pro-phagocytic signals that mediate cell uptake in these cases, are unknown, but may be uncovered using the screening platform we have established in this work.

Future biochemical identification of APMAP's endogenous substrates and evaluation of their relevance to ADCP regulation will clarify the mechanism by which APMAP regulates ADCP in a GPR84-dependent manner. Intriguingly, the list of known paraoxonase substrates partly overlaps with the list of known GPR84 agonists, as both can recognize medium chain hydroxy fatty acids[11,12]. Because Rac activation is sufficient to drive the formation of the pseudopods that mediate target cell engulfment[13] and is a critical regulated step in the initiation of phagocytosis[8], the role we establish for the Rac1 GEF PREX1 in the APMAP-GPR84 axis suggests that cancer-cell APMAP may ultimately exert its effects on phagocytosis through modulation of Rac signaling (**Fig. 4f**). While these mechanistic details will require further biochemical elucidation, our studies uncover the APMAP-GPR84 axis as a novel regulator of cancer cell phagocytosis.

Supplementary References

1. Morgens, D. W. *et al.* Genome-scale measurement of off-target activity using Cas9 toxicity in high-throughput screens. *Nat. Commun.* **8**, 15178 (2017).
2. Ralph, P. & Nakoinz, I. Phagocytosis and cytolysis by a macrophage tumour and its cloned cell line. *Nature* **257**, 393–394 (1975).
3. Chavez, A. *et al.* Highly efficient Cas9-mediated transcriptional programming. *Nat. Methods* **12**, 326–328 (2015).
4. Horlbeck, M. A. *et al.* Compact and highly active next-generation libraries for CRISPR-mediated gene repression and activation. *Elife* **5**, (2016).
5. Loureiro, L. R. *et al.* Challenges in Antibody Development against Tn and Sialyl-Tn Antigens. *Biomolecules* **5**, 1783–1809 (2015).
6. Sewell, R. *et al.* The ST6GalNAc-I sialyltransferase localizes throughout the Golgi and is responsible for the synthesis of the tumor-associated sialyl-Tn O-glycan in human breast cancer. *J. Biol. Chem.* **281**, 3586–3594 (2006).
7. Haney, M. S. *et al.* Identification of phagocytosis regulators using magnetic genome-wide CRISPR screens. *Nat. Genet.* **50**, 1716–1727 (2018).
8. Flannagan, R. S., Jaumouillé, V. & Grinstein, S. The cell biology of phagocytosis. *Annu. Rev. Pathol.* **7**, 61–98 (2012).
9. Huang, Y., Ma, Y., Gao, P. & Yao, Z. Targeting CD47: the achievements and concerns of current studies on cancer immunotherapy. *Journal of thoracic disease* vol. 9 E168–E174 (2017).
10. Perez, C. J., Dumas, A., Vallières, L., Guénet, J.-L. & Benavides, F. Several classical mouse inbred strains, including DBA/2, NOD/Lt, FVB/N, and SJL/J, carry a putative loss-of-function allele of Gpr84. *J. Hered.* **104**, 565–571 (2013).
11. Connelly, P. W. *et al.* Mouse serum paraoxonase-1 lactonase activity is specific for medium-chain length fatty acid lactones. *Biochim. Biophys. Acta* **1811**, 39–45 (2011).

12. Wang, J., Wu, X., Simonavicius, N., Tian, H. & Ling, L. Medium-chain fatty acids as ligands for orphan G protein-coupled receptor GPR84. *J. Biol. Chem.* **281**, 34457–34464 (2006).
13. Castellano, F., Montcourrier, P. & Chavrier, P. Membrane recruitment of Rac1 triggers phagocytosis. *J. Cell Sci.* **113 (Pt 17)**, 2955–2961 (2000).

Supplementary Figure 1

Extended Data Fig. 5b

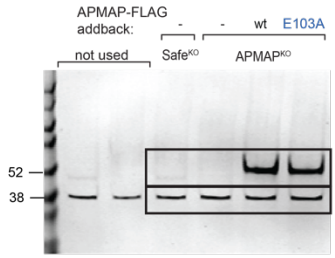

APMAP blot, followed by probing with GAPDH

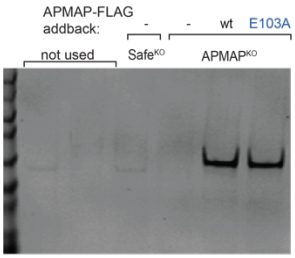

APMAP blot, prior to probing with GAPDH, for reference

Extended Data Fig. 5e

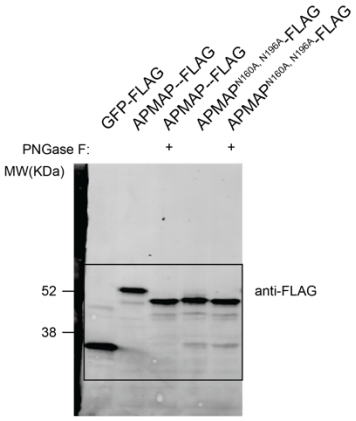

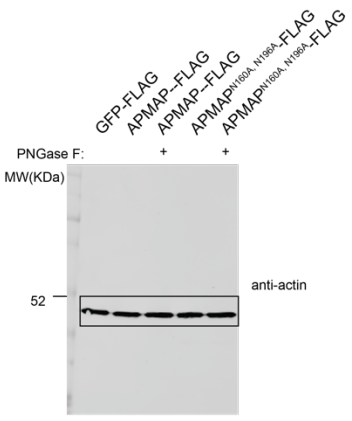

Extended Data Fig. 6a

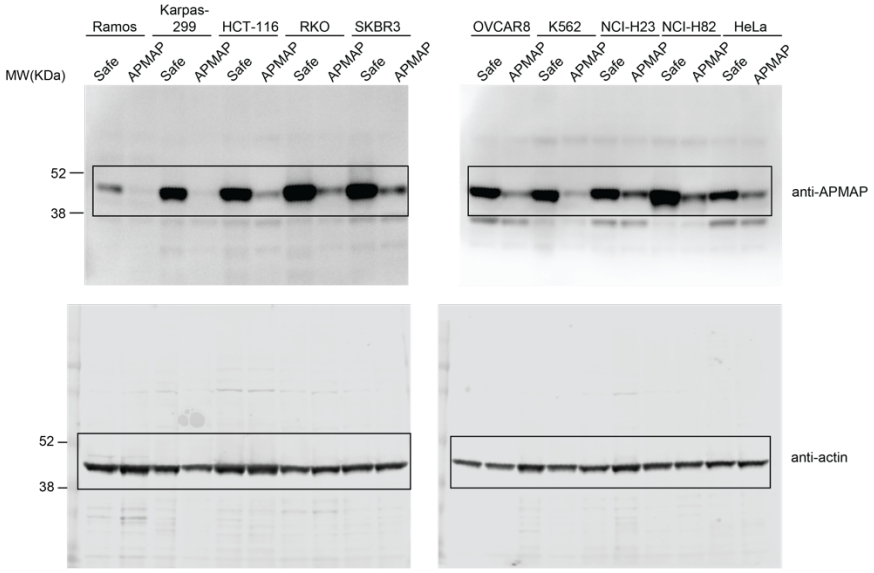

Supplementary Table Descriptions

Supplementary Table 1. RNA sequencing data for J774 macrophages with p-values from two-tailed Wald test, adjusted for multiple comparisons with Benjamini-Hochberg correction. n = 3 biologically independent samples for each condition.

Supplementary Table 2. Genome-wide ADCP CRISPR knockout screen in Ramos lymphoma cells in presence of anti-CD20. *P*-values were determined by permuting the gene-targeting guides in the screen and comparing to the distribution of negative controls using casTLE, and a 5% FDR threshold was used to defining hits using the Benjamini-Hochberg procedure. Two biologically independent screen replicates.

Supplementary Table 3. Batch re-test ADCP CRISPR knockout screen in Ramos lymphoma cells in presence of anti-CD20. Genes were noted as hits when their combination effect score at 95% credible interval did not include zero. Two biologically independent screen replicates.

Supplementary Table 4. Genome-wide ADCP CRISPR activation screen in Ramos lymphoma cells in presence of anti-CD20 and anti-CD47. *P*-values were determined by permuting the gene-targeting guides in the screen and comparing to the distribution of negative controls using casTLE, and a 5% FDR threshold was used to define hits using the Benjamini-Hochberg procedure. Two biologically independent screen replicates.

Supplementary Table 5. ADCP CRISPR knockout screen in Ramos lymphoma cells in presence of anti-CD20, +/- anti-CD47, and in sgSafe and sgCD47 genetic backgrounds, using transmembrane protein enriched sub-library. *P*-values were determined by permuting the gene-targeting guides in the screen and comparing to the distribution of negative controls using casTLE, and a 5% FDR threshold was used to define hits using the Benjamini-Hochberg procedure. Two biologically independent screen replicates in each screen.

Supplementary Table 6. Genome-wide IgG-bead phagocytosis magnetic CRISPR knockout screen in J774 macrophages. *P*-values were determined by permuting the gene-targeting guides in the screen and comparing to the distribution of negative controls using casTLE, and a 5% FDR threshold was used to defining hits using the Benjamini-Hochberg procedure. Two biologically independent screen replicate screens were conducted but one unbound replicate had insufficient coverage so only one unbound replicate was compared to both of the bound replicates.

Supplementary Table 7. Genome-wide ADCP FACS CRISPR knockout screen in J774 macrophages for uptake of $Safe^{KO}$ and $APMAP^{KO}$ Ramos cells. *P*-values were determined by permuting the gene-targeting guides in the screen and comparing to the distribution of negative controls using casTLE, and a 5% FDR threshold was used to define hits using the Benjamini-Hochberg procedure. Two biologically independent screen replicates.

Supplementary Table 8. ADCP FACS CRISPR knockout screen in J774 macrophages for uptake of Safe^{KO} and APMAP^{KO} Ramos cells, using phagocytosis regulator-enriched sublibrary. *P*-values were determined by permuting the gene-targeting guides in the screen and comparing to the distribution of negative controls using casTLE, and a 5% FDR threshold was used to define hits using the Benjamini-Hochberg procedure. Two biologically independent screen replicates.

Supplementary Table 9. sgRNA sequences used in this study.